ACS NANO

www.acsnano.org

ARTICLE

Surface Ligands Dictate the Mechanical Properties of Inorganic Nanomaterials

Sarah M. Rehn, Theodor M. Gerrard-Anderson, Yu Chen, Peng Wang, Timothy Robertson, Thomas P. Senftle, and Matthew R. Jones*

Cite This: *ACS Nano* 2023, 17, 6698–6707

Read Online

ACCESS | Metrics & More | Article Recommendations | Supporting Information

ABSTRACT: **The ability for organic surface chemistry to influence the properties of inorganic nanomaterials is appreciated in some instances but is poorly understood in terms of mechanical behavior. Here we demonstrate that the global mechanical strength of a silver nanoplate can be modulated according to the local binding enthalpy of its surface ligands. A continuum-based core−shell model for nanoplate deformation shows that the interior of a particle retains bulk-like properties while the surface shell has yield strength values that depend on surface chemistry. Electron diffraction experiments reveal that, relative to the core, atoms at the nanoplate surface undergo lattice expansion and disordering directly related to the coordinating strength of the surface ligand. As a result, plastic deformation of the shell is more difficult, leading to an enhancement of the global mechanical strength of the plate. These results demonstrate a size-dependent coupling between chemistry and mechanics at the nanoscale.**

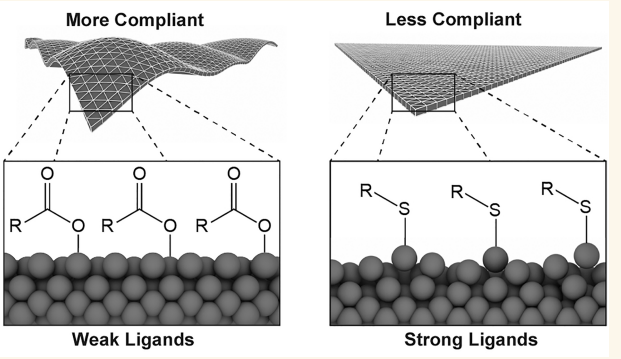

KEYWORDS: *nanoplate, surface chemistry, nanomechanics, chemomechanics, electron microscopy, ligand exchange*

Nanoscience is built on the principle that unique properties arise at small length scales. Such phenomena can develop from a wide variety of factors including quantum confinement, changing reactivity, or an increased proportion of surface atoms. For example, optical properties arise in quantum dots from size-dependent coupling between photons and excitons, while catalytic behavior can be explained by the coupling of crystal size/shape and surface energy.[1−6] It is well-known that the mechanical behavior of inorganic materials is also heavily size-dependent,[7] where the elastic deformation of a structure has a power law dependence on material thickness. This implies that, for sufficiently small systems, mechanical behavior may couple to other physical factors whose influence would be trivial for materials at macroscopic scales.

Although historically the identity of surface ligands on nanomaterials has been considered mostly in the context of colloidal stability and functionalization,[8,9] there is a growing appreciation for the ability of ligands to influence or even dictate certain properties. For example, it has been observed that surface ligands can change the photoluminescent performance of quantum dots (QDs) and noble metal nanoclusters by eliminating surface traps and reducing nonradiative relaxation pathways.[10−12] It has also been shown that exchanging ligand chemistries can change the crystallographic phase of thin gold nanosheets and modulate interatomic distances in metal nanoparticles and nanoclusters.[13−21] Although additional scholarly work over the past several decades has shown that the chemistry of surface ligands can have a major impact on the bonding and atomic structure at inorganic surfaces, the connection between these processes and global mechanical response remains underexplored and poorly understood.

The physical consequences of organic ligand adsorption to metal surfaces have been investigated primarily by two scientific communities—molecular sensing and surface science. The former studies the bending of microcantilevers in response to adsorbate binding—an effect attributed to changes in surface stress, or the work required to elastically stretch a surface. This understanding derives from a continuum-scale perspective that, by definition, does not include the details of atomic reorganization and chemisorption.[22−34] The latter community experimentally probes angstrom-level shifts in

Received: December 16, 2022
Accepted: March 20, 2023
Published: March 27, 2023

atomic positions in bare and decorated surfaces, but generally does not connect these processes to the global mechanical properties of a material.[35−43] Understanding ligand-driven mechanics in inorganic structures at the nanoscale represents an opportunity to reconcile the observations made in each of the previously described fields since nanoscience is uniquely positioned in an intermediate size regime between the atomic and macroscale.

RESULTS AND DISCUSSION

In this work we show that the chemistry of surface ligand adsorption, a ubiquitous phenomenon in colloidal nanoscience, controls the global mechanical properties of nanoparticles with at least one dimension below ∼20 nm. This effect arises from the ability of a surface-bound molecule to alter the sign and magnitude of intrinsic surface stress in a nanocrystal. Nanoscale systems are ideal for interrogating this phenomenon, as the role of surface chemistry is enhanced due to the increased ratio of surface-like to bulk-like atoms.[44−47] It is observed that nanoplates bound by strongly interacting ligands display a greater mechanical strength than their counterparts with weakly interacting ligands (Figure 1). We show that this shift in mechanical properties is a direct consequence of the surface stress induced by the atomic disordering of surface atoms upon ligand interaction. These results challenge the conventional depiction of nanoparticles as static, rigid objects and instead demonstrates their ability to be mechanically transformed via surface chemistry.

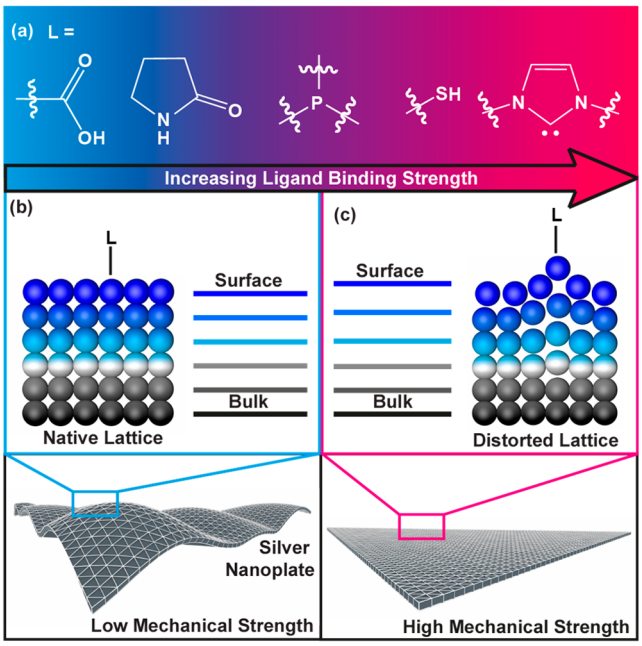

Figure 1. Control of silver nanoplate mechanical behavior with surface chemistry. (a) Inorganic surfaces are often decorated with small molecule ligands (L) that can present a variety of different binding chemistries. (b) Weakly binding ligands have less impact on the atomic lattice at the surface, resulting in a nanoplate that displays low mechanical strength. (c) Ligands that bind more strongly to the silver surface induce atomic distortions that result in an increase in the global mechanical strength of the nanoplate. Atoms are colored with a gray-to-blue gradient indicating the gradual departure from bulk-like behavior of a surface cross section.

Deformation of Ultrathin Nanoplates Elucidates Chemo-Mechanical Coupling. To explore the impact of surface ligand chemistry on nanoscale mechanical behavior, we optimized the synthesis of ultrahigh aspect ratio triangular silver nanoplates of ∼8 nm in thickness and hundreds of nanometers on-edge (Figure 1b−c). Previous work has demonstrated that nanoplates of these dimensions are extraordinarily flexible and can be plastically deformed over small spherical template particles in a controllable manner (Figure 2a, Table S1).[48] Transmission electron microscopy (TEM) can be used to observe this deformation through the appearance of bend contours, the dimensions of which can be used to extract effective mechanical constants (Figure 2b).[48]

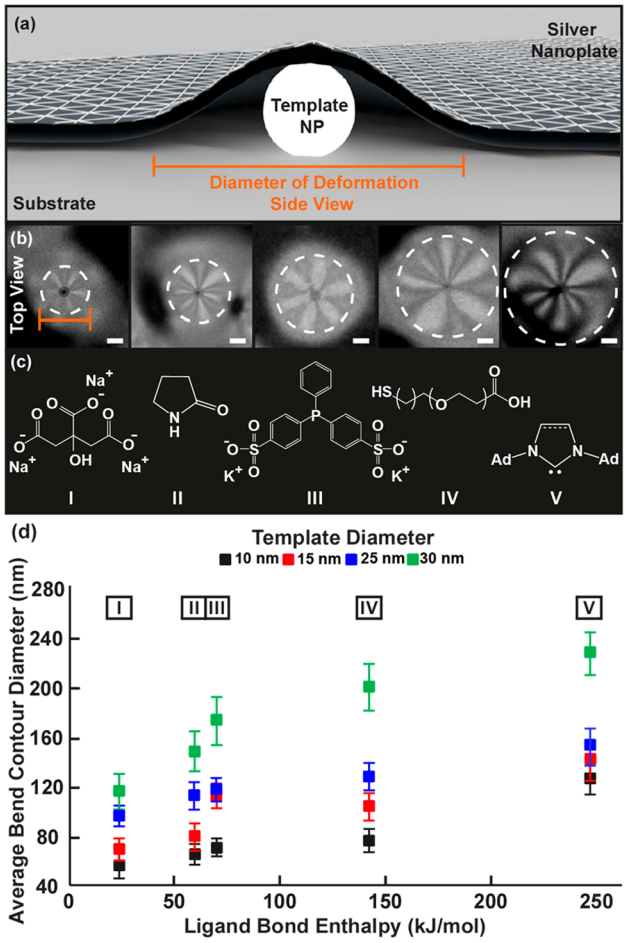

Figure 2. TEM-based investigation of silver nanoplate deformation as a function of surface ligand chemistry. (a) Thin silver nanoplates are readily deformable over small spherical template particles, generating a distinctive bend contour in TEM images, the diameter of which correlates to the lateral extent of the deformation. (b,c) Nanoplates can be decorated with a wide range of commonly used ligands of increasing bond strength, resulting in an increase in the bend contour diameter for a single template particle size. Ligand molecules: I - citrate, II - pyrrolidone, III - bis(*p*-sulfonatophenyl)phenylphosphine (BSPP), IV - carboxylic acid terminated oligo(ethylene)glycol thiol (PEG-SH), and V - adamandtyl substituted *n*-heterocyclic carbene (NHC). (d) Ligand bond enthalpy versus average bend contour diameter reveals a proportional relationship that holds true for several template particle sizes, 10−30 nm. The tabulation of these data is available in the Supporting Information.

https://doi.org/10.1021/acsnano.2c12497
ACS Nano 2023, 17, 6698−6707

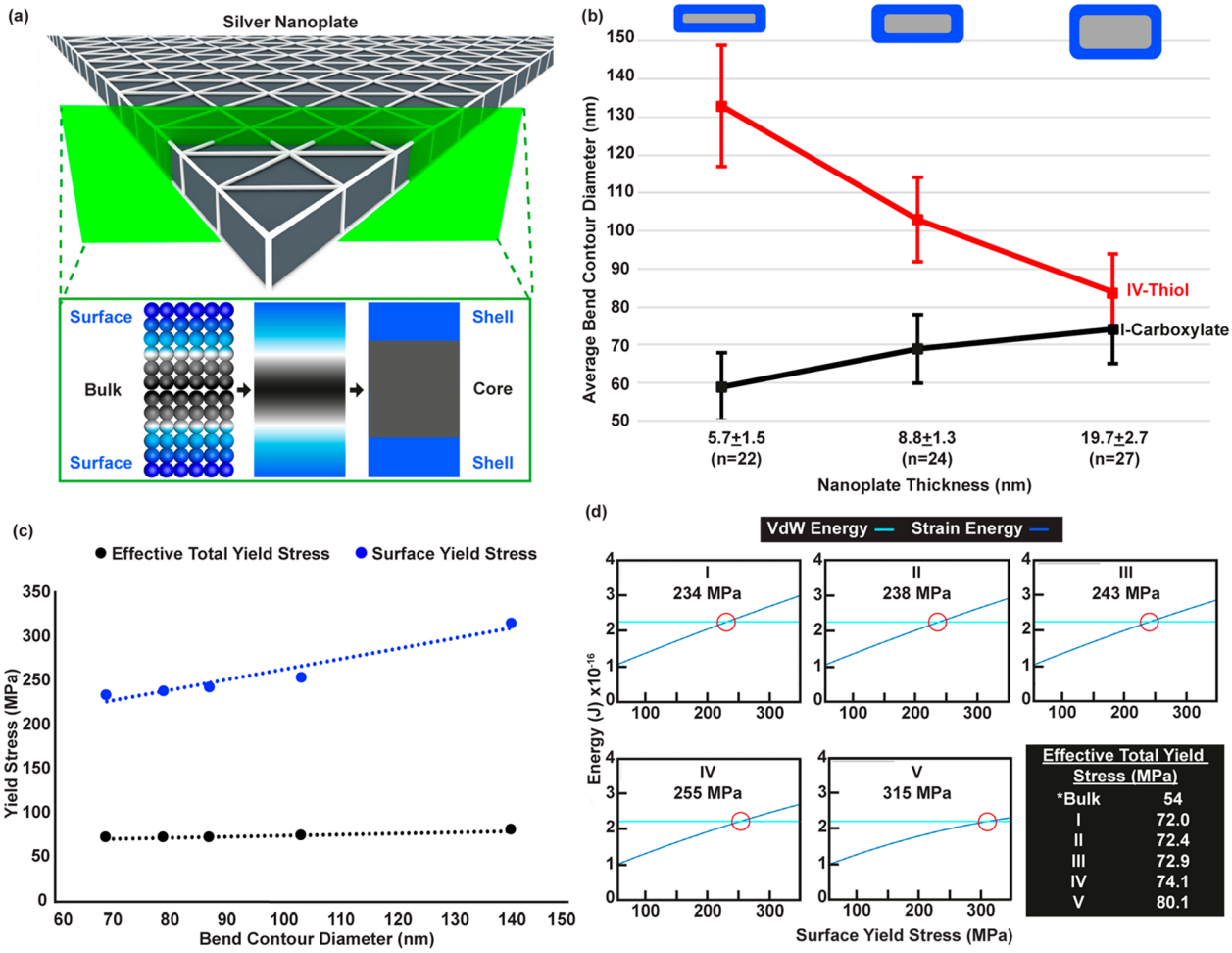

Figure 3. Core−shell modeling of ligand-decorated nanoplates. (a) Silver nanoplates can be understood as a core−shell structure, where surface (shell) atoms have mechanical properties that are susceptible to surface chemistry influences. (b) This is experimentally supported by TEM bend contour measurements demonstrating that thinner nanoplates (with a greater fraction of surface atoms) are more sensitive to changes in the ligand chemistry. (c) A continuum mechanics model for plate deformation allows for the fitting of experimental bend contours to extract mechanical constants for the surface (blue data points) compared to the plate as a whole (black data points). (d) Calculation of surface yield stress values by comparing the total strain energy of the core−shell plate to its van der Waals attraction to a substrate.

Indeed, Ag is a good candidate material for these studies due to its ductility and low cohesive energy.[49,50] In this experimental geometry, an increasing bend contour size indicates nanoplates of increasing mechanical strength. As such, these bend contours allow for a high-throughput and convenient method to screen the coupling of surface ligand chemistries to nanoparticle mechanics.

As synthesized, the nanoplates are capped with a weakly bound citrate ligand that can undergo facile exchange reactions with stronger binding ligands. This feature was exploited to generate a library of nanoplates decorated with various surface chemistries (Figure 2c). The ligands used in this study will be subsequently referred to by their surface-coordinating moiety: carboxylate (I), pyrrolidone (II, monomer of PVP), phosphine (III), thiol (IV, PEG-SH), and carbene (V, NHC). We have included exact chemical details for all ligands used in this study, including salts and counterions, in the Methods section of this manuscript. Interestingly, when plastically deformed over spherical template particles, the diameter of bend contours increases with the interaction strength of the nanoplate surface ligand.[43,51−54] This trend was consistent across hundreds of TEM measurements (Figures 2c, d, S1−S2, Table S2). While the ligands shown represent a library of commonly used species and their subunits (Figure 2c), we additionally performed experiments with identical R groups (pentane) while varying only the surface coordinating group (carboxylate, amine, thiol, Figures S3−S4). These data also demonstrated an increase in bend contour size with ligand−surface interaction strength. Additionally, changing the substrate composition as well as template particle composition and surface chemistry does not impact the observed behavior (Figures S5−S6). These results are to be expected due to the trivial influence of the changing Hamaker constant on the overall van der Waals interaction, and small interaction area between the template particle and the nanoplate, respectively.[48] Since a larger bend contour size indicates a nanoplate with greater mechanical strength, we can conclude from these data that some property of the surface chemistry couples to the mechanical behavior of the inorganic particle. This observation is corroborated by AFM characterization, which illustrates topographically that the lateral extent of the bend contour is directly related to the ligand binding strength (Figure S7).

https://doi.org/10.1021/acsnano.2c12497
ACS Nano 2023, 17, 6698−6707

These observations are consistent with recent work that demonstrated cantilever deflection as a function of adsorbate interaction strength.[32]

To determine the role that ligand coordination plays on nanoplate mechanics, we considered several potential influences. For instance, it has been previously shown that submonolayer coverage of ligands on metal surfaces can induce surface stresses as a result of lateral side-chain interactions.[24,30,55−57] Therefore, we quantified the packing densities of each ligand studied using inductively coupled plasma (ICP) mass spectrometry (MS) to determine the concentration of silver nanoplates and thermogravimetric analysis (TGA) to measure ligand molecule concentrations. These data were used to calculate an areal footprint specific to each surface chemistry: 3.4 ± 0.1, 4.9 ± 0.4, 3.0 ± 0.2, and 3.9 ± 0.1 molecules/nm^2 for carboxylate, pyrrolidone, phosphine, and thiol ligands, respectively (Figures S8, S9, Table S3, Scheme S1); carbene functionalized particles could not be generated in high enough quantities for TGA analysis, therefore yielding no density information. These measured surface densities are consistent with the maximum observed for similar compounds,[53] allowing us to conclude that none of the ligand chemistries result in submonolayer coverage. Furthermore, these measurements only varied in magnitude by at most 60% and lacked any trend following the observed mechanical behavior, suggesting that ligand density alone cannot explain the increased nanoplate strength. We then examined the influence that ligand side-chain interactions might play in dense monolayers by functionalizing plates with molecules that have the same surface coordinating group but varying substituents. For plates modified with thiol-based ligands having variable alkyl, ethylene glycol, or crown-ether moieties, there was no statistical difference in bend contour diameters, indicating no effect on nanoplate mechanics (Figure S10). This finding is significant, as side chains bearing these chemistries experience different van der Waals interactions.[53,58] We note that thiol ligands with variable alkyl and ethylene glycol lengths will have similar surface packing behavior and density, but the packing enthalpy will increase with chain length.[53] These data demonstrate that there is no effect on nanoplate mechanics based solely on the interactions due to side chain packing or side chain length. Additionally, we expect that the thiol ligand bearing the crown ether moiety will have a larger packing footprint than the former group of ligands due to steric hindrance from the bulky ring. However, in this case, the observed mechanical behavior is again the same. In a more extreme case, experiments performed where nanoplates are decorated with a long polymer of pyrrolidone, PVP29, demonstrated the same bend contour sizes as the pyrrolidone monomer (Table S2). From these data, we conclude that, in the regime of full monolayer coverage, neither ligand−ligand interactions nor ligand density are appreciable factors in dictating nanoplate mechanics. As a result, we focus on the role of the coordinating strength of the surface ligand.

A Core−Shell Model for Ligand-Mediated Mechanical Behavior. Based on the experimental data, it is apparent that a local atomic interaction at the ligand−nanoplate interface results in mutable global mechanical behavior. This suggests that the ligand-decorated nanoplate may be interpreted as a core−shell structure, where interior core atoms display bulk-like mechanical constants and exterior surface atoms display mechanical properties that are ligand-dependent (Figure 3). Since previous experiments demonstrated side chain composition had no impact on mechanical behavior, we approximate the shell to consist only of the first few atomic layers of silver atoms at the nanoplate surface.[42] It should be noted that this approximation is likely invalid in cases of sparse ligand decoration on a metal surface wherein factors such as side chain interactions would become more influential to the overall behavior of the system. If the core−shell geometry is a valid interpretation of the system, then the mechanical response to surface chemistry should be size dependent, i.e. changing the thickness of the nanoplate does not change the surface atom-ligand interaction but does change the relative fraction of core atoms. To test this, nanoplates of different thicknesses were synthesized and plastically deformed over template particles for the cases of carboxylate and thiol ligand chemistries (Figure 3b). For each nanoplate thickness, the general trend with changing surface chemistry holds true: thiol-capped nanoplates produce a larger bend contour than their carboxylate-capped counterparts. However, the magnitude of the effect increases as nanoplates become thinner, indicating that surface atoms bound by strong ligands produce shells that are mechanically stronger than the bulk-like core. As expected, the data show an asymptotic behavior as nanoplate thickness increases and demonstrate that beyond a thickness of 20 nm the effect of the ligand-dependent shell is rendered negligible. These findings also clearly demonstrate that this behavior is truly a nanoscale effect, brought about by the unique environment of the surface and its outsized influence on the overall behavior of the system.

To gain further insight into how the shell atoms modulate the effective mechanical behavior of the entire nanostructure, we modified an analytical model developed in our previous work that compares the strain energy of a plate against its van der Waals attraction to a substrate.[48] More specifically, a radially symmetric solution to the Kirchhoff−Love equations for the deformation of a plate was modified to account for both plastic deformation and a core−shell geometry (see Supporting Information); the core is assigned the bulk properties of Ag, and the shell has mechanical constants that are allowed to vary in order to match the observed bend contour dimensions. This analysis shows that experimentally consistent bend contours can only be generated in the model if the yield stress of the shell material (not the elastic modulus) increases with ligand binding strength,[48] adopting values ranging from 234 to 315 MPa (Figure 3c−d), which is significantly higher than the bulk yield stress of silver, 54 MPa (see Supporting Information). This accounts for a difference in the overall yield stress of the plate of 72 to 80 MPa, even for a particle consisting of dozens of atomic layers in thickness (∼9 nm, Figure 3c, d). While it is probable that the Young's modulus is also affected by ligand chemistry and size effects,[26,59] the contribution from elastic deformation is negligible under the existing experimental conditions, accounting for <10% of the overall strain energy in the system. Consequently, this demonstrates that chemo-mechanical coupling at the surface of an inorganic nanostructure is size dependent and dominated by changes to the effective yield stress of surface atoms.

Characterizing Lattice Distortions at the Ligand−Surface Interface. It is well appreciated that ligand binding to inorganic surfaces results in atomic restructuring and changes to surface stress.[42] Most bare metal surfaces experience both in- and out-of-plane lattice contraction due to under-coordination and are defined to be under an intrinsic tensile surface stress. Adsorption of surface ligands relaxes this surface stress due to atomic reorganization. For interactions of

https://doi.org/10.1021/acsnano.2c12497
ACS Nano 2023, 17, 6698−6707

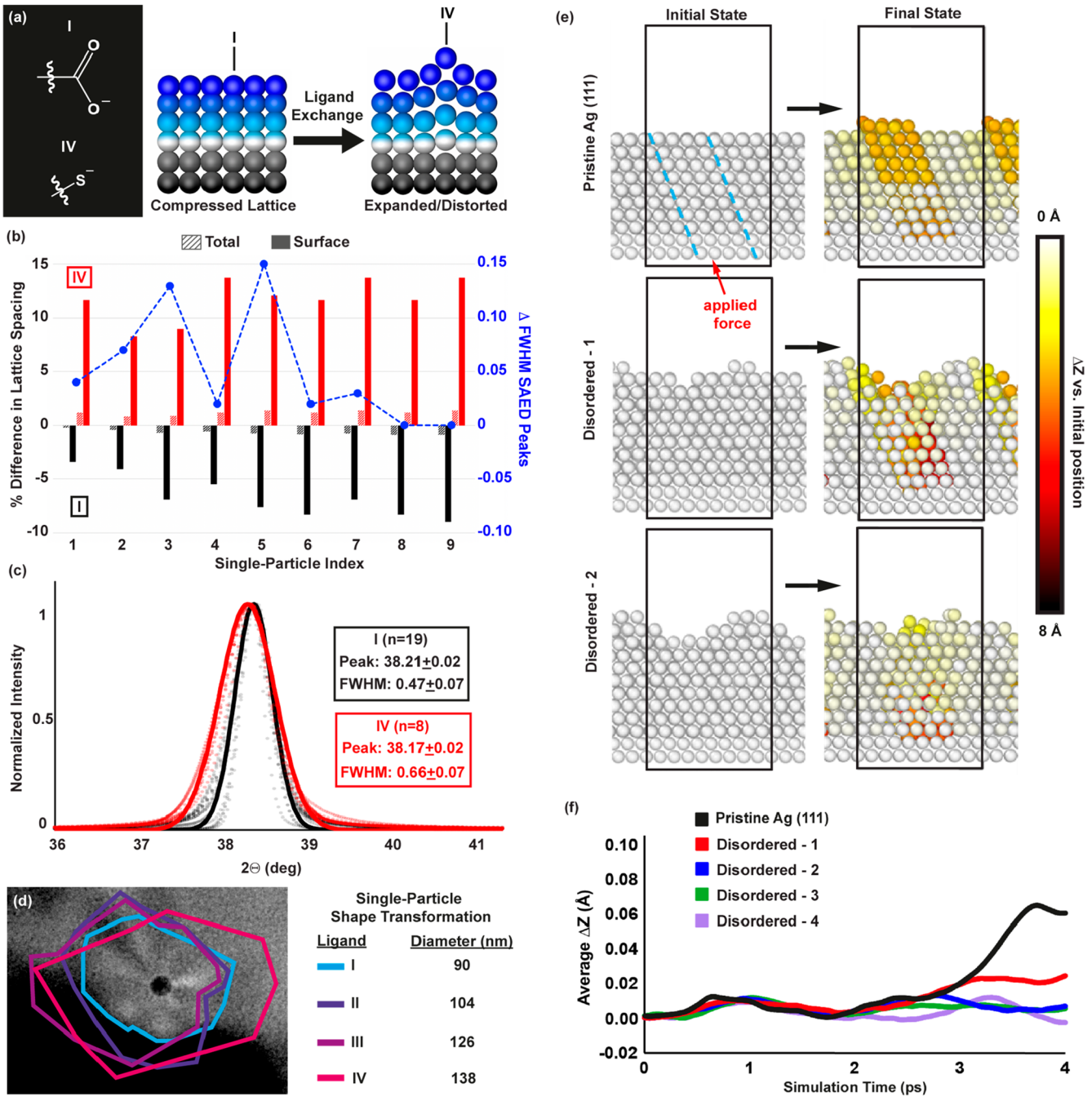

Figure 4. Ligand mediated atomic distortion and mechanical behavior of distorted Ag surfaces. (a) Upon decoration with a strongly binding thiol ligand (I:IV ligand exchange), atoms in the silver nanoplate lattice expand and are distorted from their original positions. (b) Correlated, single particle TEM measurements demonstrate the transformation in lattice spacing that occurs in undeformed nanoplates upon exchange from carboxylate to thiol surface chemistry. Black bars represent lattice spacing compared to bulk silver for carboxylate capped plates, and red bars show the lattice expanded after exchange with thiol ligands. Blue data points represent the Δfwhm of peaks in SAED data both before and after ligand exchange, showing that, for most individual plates, the silver lattice becomes distorted in addition to expanding. These observations are further confirmed by (c) bulk XRD data showing a peak shifting and broadening corresponding to lattice expansion and distortion, respectively, upon ligand exchange. (d) Correlated TEM imaging after successive ligand exchange reveals an increase in bend contour size, shown in a colored outline overlaid with the original carboxylate (I) TEM image. (e) MD simulation snapshots showing initial and final structures of the Ag slab model for a pristine Ag (111) surface and two of several disordered structures (others are shown in the SI). (f) A plot of the average ΔZ of the topmost 32 atoms located in the area of the applied force, plotted as a function of simulation time. See Supporting Information for further details.

increasing strength, this reorganization involves lattice expansion and the introduction of surface compressive stresses and can even remove atoms from the material.[42] These surface effects not only impact the primary surface atoms but also cause distortions propagating inward two to four atomic layers (Figure 4).[42] To probe this effect, we collected selected area electron diffraction (SAED) data of undeformed single nanoplates before and after ligand exchange (Figures 4b,

https://doi.org/10.1021/acsnano.2c12497
ACS Nano 2023, 17, 6698−6707

S11, Table S4). Since surface atoms make up a non-negligible percentage of thin nanoplates (≥10%), lattice measurements from electron diffraction patterns for an entire particle should show deviations from the expected value if large surface reorganizations exist. Correlated lattice measurements were obtained for nine individual nanoplates capped first with carboxylate ligands (black) and then exchanged to thiol ligands (red, Figure 4b). On average, carboxylate-capped nanoplates exhibited a lattice contraction of 6.7%. This value is consistent with minor relaxation of surface stress by a weakly bound physiosorbed ligand since bare metal surfaces are known to have lattice contractions of up to 15%, resulting in tensile surface stresses of approximately 4 N m^{-1}.[35,40,42] Once exchanged with thiol ligands, the nanoplates have an average lattice expansion of 11.8%, which is in good agreement with literature studies that have seen thiol-mediated expansions of up to 19% and resulting compressive surface stresses of −5 N m^{-1}.[15,39] While the orientation of the electron beam with respect to the nanoplate in SAED measurements can only capture the in-plane lattice distortions, out-of-plane stresses of the same direction and magnitude are known to occur and are consistent with our results.[42] Importantly, analysis of the full width at half-maximum (fwhm) of the SAED peaks reveals broadening for most of the particles studied, indicating a disordering of the surface atoms that is concomitant with the lattice expansion driven by ligand binding (Figure 4b). These single-particle data are corroborated by bulk X-ray diffraction (XRD) measurements of nanoplates assembled into [111]-oriented films, which also show peak shifting and broadening in thiol-capped samples corresponding to lattice expansion and surface atom disordering (Figures 4c, S12). We note that while there have been many studies on inorganic surface reconstructions as a function of surface molecular interactions, these are usually performed on ultraclean bare metal surfaces. In addition, the nanoplates used in this work are bound predominantly by {111} facets, which are the lowest energy and most densely packed in FCC crystals and therefore experience minimal driving force for reconstructing at room temperature. Directly measuring surface reconstructions on colloidal nanoparticles is challenging, and the data presented showing lattice distortion for two extreme cases (weakly binding carboxylate and strongly binding thiol ligands, Figure 4b) exist close to the limit of quantitation of the techniques employed. Although it is possible that changing the binding strength and the denticity of the surface ligands will induce different surface reconstructions, this is unlikely for FCC {111} and is not indicated by our data, given the resolution limitations of our measurements. Disambiguating these variables is nontrivial and is a topic for future investigations into this phenomenon.

Role of Surface Disorder in Material Strength. These experiments establish that, before being deformed, nanoplates with strongly bound ligands consist of a "shell" of surface atoms that are expanded and disordered relative to the core and/or nanoplates with more weakly bound ligands. Separately, a continuum mechanics model has shown that the increased overall strength of a nanoplate can only be explained by increases to the yield stress of the shell. Because plastic deformation typically occurs through atom or dislocation motion along preferred crystallographic directions called slip systems, we hypothesize that the mechanism of ligand-dependent nanoplate mechanics arises from the disruption of slip planes due to ligand-induced disordering of surface metal atoms. Indeed, previous literature has demonstrated that amorphous metallic glasses formed via ultrafast cooling have increased yield stresses compared to their crystalline counterparts due to disrupted deformation modes.[60,61] To determine if ligand-induced disorder can diminish mechanical compliance, we performed molecular dynamics (MD) simulations to understand the relationship between surface disorder and yield strength. We constructed models of a disordered surface from a high-temperature melting and quenching procedure (see Methods) that was repeated using varying temperature conditions to sample a range of possible disordered atomic configurations. We simulated particle deformation by applying a constant external force to the bottom of the Ag slab along the slip plane (Figure 4e). The average position change in the z coordinate of the topmost atoms in the projected region of the applied external force was monitored over the course of the MD simulations (Figure 4f). If the applied force cannot induce movement of the atoms along the slip plane, then the material is more mechanically stiff, resulting in a larger bend contour diameter measured in experiments. While atoms readily move along the slip plane when the force is applied to the ordered Ag (111) surface model, there is very little movement of surface atoms when the same external force is applied to the disordered Ag surface models (Figure 4e, f). These findings support the notion that ligand-induced surface disorder inhibits plastic deformation along slip systems.

Changing Nanoplate Shape with Surface Chemistry. Another important facet of this observation is the potential to utilize ligand chemistry to dynamically change the shape of a nanostructure (Figure 4d). To demonstrate this, a correlated single-particle TEM analysis was performed on template-deformed nanoplates that were sequentially incubated in solutions of increasingly strong ligands and imaged after each iteration (Figure 4d). As expected, the bend contour size increased after each progressive step of the ligand exchange as the nanoplates became less mechanically compliant, corresponding to a change in the physical shape of a nanoplate as a function of ligand chemistry alone (Figures 4d, S13). This observation was consistent across several different examples of bend contours and demonstrates that surface chemistry can be a powerful tool for dynamic structural control of inorganic nanomaterials.

CONCLUSIONS

This work links atomic-scale ligand-surface interactions with global mesoscale changes in the mechanical properties of a material. Nanoscale objects, which reside at an intermediate regime between these length scales, are particularly sensitive to these effects and are therefore distinctly situated to study this phenomenon. These results also show that ligand-based chemomechanical coupling is a size-dependent nanoscale property, occurring only for structures whose proportion of surface atoms is sufficiently high, ∼10%. Our findings are striking, since colloidal nanomaterials have been stabilized by surface ligands for decades without a complete understanding of the mechanical consequences of this interaction. The traditional notion of nanoparticles as rigid, static objects must therefore be re-evaluated, as their ability to reshape dynamically upon changes in their surface chemistry is evident. These fundamental results will further impact the interpretation of experiments on the immense array of inorganic materials that have properties sensitive to surface structure.

https://doi.org/10.1021/acsnano.2c12497
ACS Nano 2023, 17, 6698−6707

METHODS

Chemicals and Materials. All chemicals were used as purchased with no further purification or processing. Trisodium citrate ($Na_3C_6H_5O_7{\cdot}2H_2O$, 99.0% ACS Reagent), silver nitrate ($AgNO_3$, 99.9999% trace metals basis), hydrogen peroxide (H_2O_2, 30% w/w in water ACS reagent with inhibitor), sodium borohydride ($NaBH_4$, 99.99% trace metals basis), L-ascorbic acid ($C_6H_8O_6$, 99.0% bioXtra), hydrochloric acid (HCl, >99.999%), nitric acid (HNO_3, >99.999%), deuterium oxide (D_2O, 99.9%), 2-pyrrolidone (C_4H_7NO, ≥99%), Silver standard for ICP (1000 mg/mL, *Trace*Cert), Holmium standard for ICP (1000 mg/mL, *Trace*Cert), Indium standard for ICP (1000 mg/mL, *Trace*Cert), 1,3-Bis(1-adamantyl)imidazolium tetrafluoroborate ($C_{23}H_{33}BF_4N_2$, 97%), and potassium *tert*-butoxide solution (KO^tBu, 1.0 M in THF) were purchased from Sigma-Aldrich. Acetonitrile (C_2H_3N, ChromAR) was purchased from Macron. The thiol molecules used for ligand studies, HS-C_x-$(PEG)_y$-COOH (x = 6,11, y = 3,6) and 12-Crown-4-CH_2-O-CH_2-SH were purchased from Prochimia Surfaces. Bis(*p*-sulfonatophenyl)phenylphosphine dihydrate dipotassium salt (BSPP, >97%) was purchased from Strem Chemicals, Inc. Oleic acid capped iron oxide nanospheres (15 nm) in chloroform were purchased from Ocean NanoTech.

Preparation of Ag Nanoplates. Silver nanoplates were prepared by modification of previously published protocols.[62,63] Seeds were prepared in an aqua regia-cleaned scintillation vial by combining fresh nanopure water (20 mL), trisodium citrate (1.2 mL, 75 mM), $AgNO_3$ (0.020 mL, 100 mM), and H_2O_2 (0.048 mL, 30% w/w) under vigorous stirring. To this, a freshly prepared solution of $NaBH_4$ (0.120 mL, 100 mM) was injected, and the reaction progressed over a 30 min as the solution turned from yellow to blue. The nanoprism seeds were stored on a benchtop at room temperature. To grow thin, high aspect ratio nanoplates, an aqua-regia cleaned scintillation vial in an ice bath, fresh nanopure water (10 mL), acetonitrile (5 mL), trisodium citrate (0.200 mL, 75 mM), and ascorbic acid (0.100 mL, 100 mM) were added under vigorous stirring. Meanwhile, an aliquot of the previously prepared seeds was subjected to centrifugation (10 min, 20133 rcf) to remove unreacted precursors. After the spin cycle, the supernatant was removed and the pelleted nanoprisms were concentrated 5× via resuspension in fresh nanopure water. These concentrated nanoplate seeds were immediately added to the reaction vial (0.035 mL), after which $AgNO_3$ (0.120 mL, 100 mM) was injected. This slow growth reaction proceeded to stir vigorously in the ice bath for approximately 2 h, yielding a pale blue solution, before being moved to the refrigerator. After growth overnight, large thin silver nanoplates had visibly settled out of solution as a gray precipitate. Upon disturbing the precipitate, the solution appeared to be blue with a gray pearlescent quality, indicating the presence of the large, light scattering nanoplates. Thicker nanoplates were achieved by adding less trisodium citrate to the growth solution. This provides less passivation of the (111) triangular faces and allows for more growth to occur along the thickness dimension. Thinner nanoprisms were achieved by adding less seed particles to the standard growth solution.

Ligand Exchange of Nanoplates. Grown nanoplates are natively capped with citrate ligands. To exchange citrate more strongly binding ligands for, a solution of the new ligand (0.100 mM final concentration) was added to nanoplates. This mixture was then subjected to constant agitation at 4 °C overnight before use. Nanoplates used immediately following this step are denoted "as-exchanged." *Ex situ* ligand exchange was performed when citrate-capped nanoplates were already deformed over template particles on TEM grids, by incubating the TEM sample in a solution of the new ligand (0.100 mM) for 4 h.

Preparation of N-Heterocylic Carbene. The preparation of the NHC ligand was performed following a published protocol.[64] The NHC precursor used for this study, 1,3-Bis(1-adamantyl)imidazolium tetrafluoroborate, was evacuated on a Schlenk line for an hour. Using a molar excess of a strong base, KO^tBu, the precursor was deprotonated over a dry ice/EtOAc bath (−78 °C). This was then used as an NHC ligand stock solution, where ex situ ligand exchange was performed with citrate-capped nanoplates. It should be noted that the subsequent ligand exchange occurs in the presence of deprotonation products including potassium salts.

Preparation of TEM and AFM Samples. Iron oxide nanospheres (0.001 mL) were freshly diluted into toluene (15 mL). Grown nanoplates were spun down (1 min) with a tabletop centrifuge, supernatant was removed, and the nanoplates were resuspended with an equal volume of nanopure water. To prepare a TEM sample, diluted iron nanoparticles (0.0035 mL) were drop cast onto a TEM grid and dried. Then, washed nanoplates (0.0065 mL) were drop cast onto the same grid and dried under vacuum. All BF, DF, and SAED TEM data were obtained with a JEOL 1230 High Contrast TEM operated at 80 kV. Size analysis from TEM images was done using ImageJ. To prepare AFM samples, diluted iron nanoparticles (0.015 mL) were drop cast onto a mica disc and dried under vacuum followed by washed nanoplates (0.030 mL). All AFM data were obtained with a Park NX20 AFM using tapping mode.

TGA Experiments. TGA analysis was performed using a Mettler Toledo/DSC 3+ system. A 30 mL volume of as-synthesized or as-exchanged nanoplates were rinsed and concentrated by centrifugation to remove excess ligands. The concentrated nanoplates were then placed in a heated TGA pan to remove excess moisture before analysis. To analyze the mass of ligands in the sample, the TGA proceeded in three stages: a heating ramp from room temperature to 120 °C at 20 °C/min, where the temperature was held for 10 min, and finally a heating ramp to 1000 °C at 10 °C/min. This resulted in a mass loss around 350 °C corresponding to the decomposition of organic molecules. This absolute mass loss was used to calculate the number of ligand molecules in 1 mL of nanoplate solution. For each ligand, three separate TGA analyses were performed and averaged to account for any experimental heterogeneity in nanoplate preparation and subsequent ligand exchange.

ICP-MS Experiments. The ICP-MS protocol used here was adapted from previous literature.[65] All analyses were carried out on a PerkinElmer NexION 300 ICP-MS using an argon flow. Ag nanoplate samples were digested using aqua regia solution prepared by mixing HCl and HNO_3 in a 3:1 ratio. This aqua regia was diluted with water to 5% and used as a matrix for the ICP-MS solutions. Digested nanoplates were diluted 2000× by volume for analysis. The concentration of silver in digested nanoplate samples was determined by comparison to a five point standard curve comprised of known Ag concentrations prepared from an ICP silver standard: 1, 5, 10, 20, 30 ppb. The standard solutions were measured five times while the unknown samples were measured three times and averaged. A flush was performed in between each of the sample measurements, and a blank was measured before and after all measurements were taken to ensure the validity of the measurements.

NMR Experiments. All NMR experiments were carried out using a Bruker 500 MHz NMR spectrometer. Validation of valeric acid exchange was performed following a previously published method.[66] Grown nanoplates capped with citrate ligands were exchanged with valeric acid (0.500 mM final concentration) followed by pH neutralization. Ligand exchange was then repeated with DTT (0.100 mM final concentration) to remove ligands from previous exchange. Nanoplates are then subjected to centrifugation to isolate the supernatant, which was then analyzed with NMR. Peaks corresponding to DTT and valeric acid were observed. Peaks corresponding to citrate were not observed, suggesting complete ligand exchange with valeric acid prior to the DTT exchange. To verify exchange between trisodium citrate and pyrrolidone, citrate-capped nanoparticles were synthesized in D_2O (100 mL scale) and subsequently washed and concentrated. This sample was then analyzed with NMR, and peaks corresponding to citrate were observed. This same process was repeated for nanoplates that had been exchanged for pyrrolidone. Pyrrolidone peaks were observed in the sample along with trace citrate peaks. The difference in intensity was used to determine the relative concentration of the ligands, and therefore the exchange completion.

XRD Experiments. Nanoprism synthesis and ligand exchange was performed as previously described. Particles were then suspended in rough monolayers at an air−water interface, transferred via

https://doi.org/10.1021/acsnano.2c12497
ACS Nano 2023, 17, 6698−6707

Langmuir−Schaefer direct contact to glass XRD substrates, and dried for 1 h. These samples were then analyzed using an XRD Rigaku SmartLab II device with a Copper K-alpha 1 radiation source. Samples were scanned using powder/film XRD settings, covering 30−100 degrees, a step rate of 0.01 degrees, and a rate of 10 degrees per minute. Rigaku SmartLab software was used to assign Ag lattice peak values. Origin software was used to fit Lorentzian curves to raw XRD data to acquire peak positions and full-width half-max values.

MD Simulation Methods. All molecular dynamics (MD) simulations were performed with the Large-scale Atomic/Molecular Massively Parallel Simulator (LAMMPS, 12 Dec 2018)[67] to investigate the relationship between surface disorder and mechanical compliance. The employed interatomic potential was a ReaxFF force field[68,69] using a Ag parameter set developed by Dulong et al.[70] All MD simulations were performed in the NVT ensemble, where a Nose−Hoover thermostat[71] was applied to maintain the desired temperature of the system (thermostat settings for each simulation are described below). A time step of 0.25 fs was used for the time integration of the Verlet equations of motion, unless otherwise noted.

For the pristine Ag surface, a (9 × 9) Ag (111) surface slab model with 10 layers was used as the simulation cell with periodic boundary conditions applied along the x and y directions. The unit cell dimensions were (26.38 Å, 26.38 Å, 43.93 Å) and (90°, 90°, 120°). The structure was equilibrated for 24.9 ps at a temperature of 300 K with the bottom two layers fixed in their bulk positions. The simulation time was determined by monitoring the system temperature and potential energy for convergence.

We applied a simulated annealing process to generate pseudodisordered surface structures that mimic the surface disorder induced by adsorbed ligands. Disordered structures were generated by melting the surface at different temperatures (1750, 1800, 1900, and 2000 K), where a temperature damping parameter of 0.25 fs was used to bring the system to equilibration at the temperature set point (taking 21.3, 20.6, 24.4, and 28.6 ps, respectively). We then quenched the melted surfaces to 300 K using a temperature damping parameter of 25 fs for the Ag (111) crystal system, which equilibrated after 120.0, 124.1, 122.5, and 99.4 ps, respectively (Figure S15). These structures are named Disordered 1−4, respectively. The experimental characterization suggests that lattice distortions caused by the ligand impact the first four atomic layers (Figure 4), so the bottom two layers of the surface were fixed allowing only eight layers to melt into a disordered structure.

To investigate the mechanical properties of different Ag systems, a constant external force of (−4.40 x, 2.54 y, 7.18 z) kcal mol^{-1} Å^{-1} aligned to the (111) slip plane was applied on a 4 × 4 domain of the bottom two layers for 4 ps at 300 K. The remaining Ag atoms in the bottom two layers were fixed. A smaller time step of 0.05 fs was employed to resolve the equation of motion in the presence of a high external force. The movement of the Ag atoms caused by the external force was compared in the different surface models to determine whether defects in the surface suppress atom motion and increase the yield strength, which correlates to decreased mechanical compliance.

ASSOCIATED CONTENT

Supporting Information

The Supporting Information is available free of charge at https://pubs.acs.org/doi/10.1021/acsnano.2c12497.

Size analysis of template nanoparticles; compiled bend contour data for all deformation studies; statistical analysis of bend contour measurements; bend contour data with additional ligands; NMR validation of nanoplate ligand exchange; bend contour data with varying template particle/substrate composition; AFM measurements of deformed nanoplates; ligand density data; thermogravimetric analysis of decorated nanoplates; correlated single-particle SAED data; XRD of bulk nanoplates with varying surface decoration; control data for correlated ex-situ ligand exchange; derivations for continuum-scale, core−shell modeling; equilibration data for MD simulations; MD simulation initial and final states for disordered cases 3 and 4; MD simulation structures (PDF)

AUTHOR INFORMATION

Corresponding Author

Matthew R. Jones − *Department of Chemistry and Department of Materials Science & Nanoengineering, Rice University, Houston, Texas 77005, United States;* orcid.org/0000-0002-9289-291X; Email: mrj@rice.edu

Authors

Sarah M. Rehn − *Department of Chemistry, Rice University, Houston, Texas 77005, United States*

Theodor M. Gerrard-Anderson − *Department of Chemistry, Rice University, Houston, Texas 77005, United States*

Yu Chen − *Department of Chemical and Biomolecular Engineering, Rice University, Houston, Texas 77005, United States*

Peng Wang − *Department of Chemical and Biomolecular Engineering, Rice University, Houston, Texas 77005, United States*

Timothy Robertson − *Department of Chemistry, Rice University, Houston, Texas 77005, United States*

Thomas P. Senftle − *Department of Chemical and Biomolecular Engineering, Rice University, Houston, Texas 77005, United States;* orcid.org/0000-0002-5889-5009

Complete contact information is available at: https://pubs.acs.org/10.1021/acsnano.2c12497

Notes

The authors declare no competing financial interest.

A previous version of this work was submitted to a preprint server: Sarah M. Rehn; Theodor M. Gerrard-Anderson; Yu Chen; Peng Wang; Timothy Robertson; Thomas P. Senftle; Matthew R. Jones. Surface Ligands Dictate the Mechanical Properties of Inorganic Nanomaterials. 2022, 10.26434/chemrxiv-2022-7htvk. ChemRxiv. https://chemrxiv.org/engage/chemrxiv/article-details/63698e0dfbfd381af3d343d6 (accessed March 15, 2023).

ACKNOWLEDGMENTS

M.R.J. would like to thank the Robert A. Welch Foundation (Grant No. C-1954), the David and Lucile Packard Foundation (Grant No. 2018-68049), and Rice University for financial support. S.M.R. would like to acknowledge financial support from a National Science Foundation Graduate Research Fellowship (No. 1842494). Y.C., P.W., and T.P.S. acknowledge support from an InterDisciplinary Excellence Award (IDEA) furnished by the Creative Ventures program at Rice University. The authors acknowledge the use of Electron Microscopy Center (EMC) at Rice University.

REFERENCES

(1) Mock, J. J.; Barbic, M.; Smith, D. R.; Schultz, D. A.; Schultz, S. Shape Effects in Plasmon Resonance of Individual Colloidal Silver Nanoparticles. *J. Chem. Phys.* **2002**, *116*, 6755−6759.

(2) Kelly, K. L.; Coronado, E.; Zhao, L. L.; Schatz, G. C. The Optical Properties of Metal Nanoparticles: The Influence of Size, Shape, and Dielectric Environment. *J. Phys. Chem. B* **2003**, *107*, 668−677.

(3) Takagahara, T.; Takeda, K. Theory of the Quantum Confinement Effect on Excitons in Quantum Dots of Indirect-Gap Materials. *Phys. Rev. B* **1992**, *46*, No. 15578.
(4) Hu, F.; Fei, Z. Recent Progress on Exciton Polaritons in Layered Transition-Metal Dichalcogenides. *Adv. Optical Mater.* **2020**, *8*, 1901003.
(5) Narayanan, R.; El-Sayed, M. A. Catalysis with Transition Metal Nanoparticles in Colloidal Solution: Nanoparticle Shape Dependence and Stability. *J. Phys. Chem. B* **2005**, *109*, 12663−12676.
(6) Alayoglu, S.; Aliaga, C.; Sprung, C.; Somorjai, G. A. Size and Shape Dependence of Pt Nanoparticles for the Methylcyclopentante/Hydrogen Ring Opening/Ring Enlargement Reaction. *Catal. Lett.* **2011**, *141*, 914−924.
(7) Patil, R. P.; Doan, D.; Aitken, Z. H.; Chen, S.; Kiani, M. T.; Barr, C. M.; Hattar, K.; Zhang, Y.-W.; Gu, X. W. Hardening in Au-Ag nano boxes from Stacking Fault-Dislocation Interactions. *Nat. Commun.* **2020**, *11*, 2923.
(8) Mirkin, C. A.; Letsinger, R. L.; Mucic, R. C.; Storhoff, J. J. A DNA-Based Method for Rationally Assembling Nanoparticles into Macroscopic Materials. *Nature* **1996**, *382*, 607−609.
(9) Jones, M. R.; Macfarlane, R. J.; Lee, B.; Zhang, J.; Young, K. L.; Senesi, A. J.; Mirkin, C. A. DNA-Nanoparticle Superlattices Formed from Anisotropic Building Blocks. *Nat. Mater.* **2010**, *9*, 913−917.
(10) Grandhi, G. K.; Arunkumar, M.; Viswanatha, R. Understanding the Role of Surface Capping Ligands in Passivating the Quantum Dots Using Copper Dopants as an Internal Sensor. *J. Phys. Chem. C* **2016**, *120* (35), 19785−19795.
(11) Pyo, K.; Thanthirige, V. D.; Kwak, K.; Pandurangan, P.; Ramakrishna, G.; Lee, D. Ultrabright Luminescence from Gold Nanoclusters: Rigidifying the Au(I)-Thiolate Shell. *J. Am. Chem. Soc.* **2015**, *137*, 8244−8250.
(12) Narouz, M. R.; Takano, S.; Lummis, P. A.; Levchenko, T. I.; Nazemi, A.; Kaappa, S.; Malola, S.; Yousefalizadeh, G.; Calhoun, L. A.; Stamplecoskie, K. G.; et al. Robust, Highly Luminescent Au_{13} Superatoms Protected by N-Heterocyclic Carbenes. *J. Am. Chem. Soc.* **2019**, *141*, 14997−15002.
(13) Fan, Z.; Huang, X.; Han, Y.; Bosman, M.; Wang, Q.; Zhu, Y.; Liu, Q.; Li, B.; Zeng, Z.; Wu, J.; et al. Surface Modification-Induced Phase Transformation of Hexagonal Close-Packed Gold Square Sheets. *Nat. Commun.* **2015**, *6*, 6571.
(14) Teranishi, T.; Hosoe, M.; Tanaka, T.; Miyake, M. Size Control of Monodispersed Pt Nanoparticles and Their 2D Organization by Electrophoretic Deposition. *J. Phys. Chem. B* **1999**, *103*, 3818−3827.
(15) Grönbeck, H.; Andreoni, W. Gold and Platinum Microclusters and Their Anions: Comparison of Structural and Electronic Properties. *Chem. Phys.* **2000**, *262*, 1−14.
(16) Schmid, G.; Corain, B. Nanoparticulated Gold: Syntheses, Structures, Electronics, and Reactivities. *Eur. J. Inorg. Chem.* **2003**, *2003*, 3081−3098.
(17) Jadzinsky, P. D.; Calero, G.; Ackerson, C. J.; Bushnell, D. A.; Kornberg, R. D. Structure of a Thiol Monolayer-Protected Gold Nanoparticle at 1.1 Å Resolution. *Science* **2007**, *318*, 430−433.
(18) Huang, Z.; Thomson, P.; Di, S. Lattice Contractions of a Nanoparticle Due to the Surface Tension: A Model of Elasticity. *J. Phys. Chem. Solids* **2007**, *68*, 530−535.
(19) Watari, M.; McKendry, R. A.; Vögtli, M.; Aeppli, G.; Soh, Y.-A.; Shi, X.; Xiong, G.; Huang, X.; Harder, R.; Robinson, I. K. Differential Stress Induced by Thiol Adsorption on Facetted Nanocrystals. *Nat. Mater.* **2011**, *10*, 862−866.
(20) Song, C.; Sakata, O.; Kumara, L. S. R.; Kohara, S.; Yang, A.; Kusada, K.; Kobayashi, H.; Kitagawa, H. Size Dependence of Structural Parameters in FCC and HCP Ru Nanoparticles, Revealed by Rietveld Refinement Analysis of High-Energy X-Ray Diffraction Data. *Sci. Rep.* **2016**, *6*, 31400.
(21) Kim, B. H.; Heo, J.; Kim, S.; Reboul, C. F.; Chun, H.; Kang, D.; Bae, H.; Hyun, H.; Lim, J.; Lee, H.; et al. Critical Differences in 3D Atomic Structure of Individual Ligand-Protected Nanocrystals in Solution. *Science* **2020**, *368*, 60−67.
(22) Fritz, J.; Baller, M. K.; Lang, H. P.; Rothuizen, H.; Vettiger, P.; Meyer, E.; Güntherodt, H.-J.; Gerber, C.; Gimzewski, J. K. Translating Biomolecular Recognition into Nanomechanics. *Science* **2000**, *288*, 316−318.
(23) Chen, G. Y.; Thundat, T.; Wachter, E. A.; Warmack, R. J. Adsorption-Induced Surface Stress and its Effects on Resonance Frequency of Microcantilevers. *J. Appl. Phys.* **1995**, *77*, 3618.
(24) Berger, R.; Delamarche, E.; Lang, H. P.; Gerber, C.; Gimzewski, J. K.; Meyer, E.; Güntherodt, J. Surface Stress in the Self-Assembly if Alkanethiols on Gold. *Science* **1997**, *276*, 2021−2024.
(25) Hu, Z.; Thundat, T.; Warmack, R. J. Investigation of Adsorption and Adsorption-Induced Stresses using Microcantilever Sensors. *J. Appl. Phys.* **2001**, *90*, 427.
(26) Godin, M.; Tabard-Cossa, V.; Grütter, P.; Williams, P. Quantitative Surface Stress Measurements Using a Microcantilever. *Appl. Phys. Lett.* **2001**, *79*, 551−553.
(27) Sander, D.; Ibach, H. Surface Free Energy and Surface Stress. *Numerical Data and Functional Relationships in Science and Technology*, Group III Condensed Matter, Vol. *42*; Springer: 2002; pp 1−49.
(28) Begley, M. R.; Utz, M.; Komaragiri, U. Chemo-Mechanical Interactions Between Adsorbed Molecules and Thin Elastic Films. *J. Mech. Phys. Solids* **2005**, *53*, 2119−2140.
(29) Lachut, M. J.; Sader, J. E. Effect of Surface Stress on the Stiffness of Cantilever Plates. *Phys. Rev. Lett.* **2007**, *99*, 206102.
(30) Desikan, R.; Armel, S.; Meyer III, H. M.; Thundat, T. Effect of Chain Length on Nanomechanics of Alkanethiol Self-Assembly. *Nanotechnol.* **2007**, *18*, 424028.
(31) Mertens, J.; Calleja, M.; Ramos, D.; Taryn, A.; Tamayo, J. Role of the Gold Film nanostructure on the Nanomechanical Response of Microcantilever Sensors. *J. Appl. Phys.* **2007**, *101*, 034904.
(32) Pinnaduwage, L. A.; Boiadjiev, V. I.; Hawk, J. E.; Gehl, A. C.; Fernando, G. W.; Rohana Wijewardhana, L. C. An Energy Conservation Approach to Adsorbate-Induced Surface Stress and the Extraction of Binding Energy Using Nanomechanics. *Nanotechnology* **2008**, *19*, 105501.
(33) Chen, C.-S.; Chou, C.-C.; Chang, S.-W. Multiscale Analysis of Adsorption-Induced Surface Stress of Alkanethiol on Microcantilever. *J. Phys. D: Appl. Phys.* **2013**, *46*, 035301.
(34) Zhao, Y.; Gosai, A.; Kang, K.; Shrotriya, P. Multiscale Modeling Reveals the Cause of Surface Stress Change onMicrocantilevers Due to Alkanethiol SAM Adsorption. *J. Chem. Inf. Model.* **2020**, *60*, 2998−3008.
(35) Jona, F.; Marcus, P. M. Surface Structures from LEED: Metal Surfaces and Metastable Phases. In *The Structure of Surfaces II*; van der Veen, J. F., Van Hove, M. A., Eds.; Springer Series in Surface Sciences, Vol. *11*; Springer: 1988.
(36) Somorjai, G. A.; Van Hove, M. A. Adsorbate-Induced Restructuring of Surfaces. *Prog. Surf. Sci.* **1989**, *30*, 201.
(37) Ibach, H. Adsorbate Induced Surface Stress. *J. Vac. Sci. Technol. A* **1994**, *12*, 2240.
(38) Starke, U.; Van Hove, M. A.; Somorjai, G. A. Adsorbate-Induced Relaxations of Close-Packed FCC and HCP Metal Surfaces. *Prog. Surf. Sci.* **1994**, *46*, 305−319.
(39) Ibach, H. The Role of Surface Stress in Reconstruction, Epitaxial Growth and Stabilisation of Mesoscopic Structures. *Surf. Sci. Rep.* **1997**, *29*, 195−263.
(40) Haiss, W. Surface Stress of Clean and Adsorbate-Covered Solids. *Rep. Prog. Phys.* **2001**, *64*, 591.
(41) Nichols, R. J.; Nouar, T.; Lucas, C. A.; Haiss, W.; Hofer, W. A. Surface Relaxation and Surface Stress of Au(111). *Surf. Sci.* **2002**, *513*, 263−271.
(42) Somorjai, G. A.; Li, Y. *Introduction to Surface Chemistry and Catalysis*; Wiley: New York, 2010.
(43) Jewell, A.; Tierney, H.; Sykes, E. C. H. Gently Lifting Gold's Herringbone Reconstruction: Trimethylphosphine on Au(111). *Phys. Rev. B* **2010**, *82*, 205401.
(44) Alberts, M. R.; Yates, J. T., Jr. *The Surface Scientist's Guide to Organometallic Chemistry*; American Chemical Society: WA, 1987.

https://doi.org/10.1021/acsnano.2c12497
ACS Nano 2023, 17, 6698−6707

(45) Schmid, G. The Relevance of Shape and Size of Au55 Clusters. *Chem. Soc. Rev.* **2008**, *37*, 1909−1930.
(46) Pei, Y.; Shao, N.; Gao, Y.; Zeng, X. C. Investigating Active Site of Gold Nanoparticle Au55(PPh3)12Cl6 in Selective Oxidation. *ACS Nano* **2010**, *4*, 2009−2020.
(47) Jin, R.; Zhu, Y.; Qian, H. Quantum-Sized Gold Nanoclusters: Bridging the Gap Between Organometallics and Nanocrystals. *Chem.—Eur. J.* **2011**, *17*, 6584−6593.
(48) Rehn, S. M.; Gerrard-Anderson, T. M.; Qiao, L.; Zhu, Q.; Wehmeyer, G.; Jones, M. R. Mechanical Reshaping of Inorganic Nanostructures with Weak Nanoscale Forces. *Nano Lett.* **2021**, *21*, 130−135.
(49) Kambe, K. Cohesive Energy of Noble Metals. *Phys. Rev.* **1955**, *99*, 419.
(50) Liu, L.; Shinozaki, K. Toughening Silica Glass by Imparting Ductility using a Small Amount of Silver Nanoparticles. *Mater. Sci. Eng., A* **2021**, *817*, 141372.
(51) Chong, G.; Laudadio, E. D.; Wu, M.; Murphy, C. J.; Hamers, R. J.; Hernandez, R. Density, Structure, and Stability of Citrate^{3-} and H_2citrate$^-$ on Bare and Coated Gold Nanoparticles. *J. Phys. Chem. C* **2018**, *122*, 28393−28404.
(52) Al-Saidi, W. A.; Feng, H.; Fichthorn, K. A. Adsorption of Polyvinylpyrrolidone on Ag Surfaces: Insight into a Structure-Directing Agent. *Nano Lett.* **2012**, *12*, 997−1001.
(53) Boles, M. A.; Ling, D.; Hyeon, T.; Talapin, D. V. The Surface Science of Nanocrystal. *Nat. Mater.* **2016**, *15*, 141−153.
(54) Lovat, G.; Doud, E. A.; Lu, D.; Kladnik, G.; Inkpen, M. S.; Steigerwald, M. L.; Cvetko, D.; Hybertsen, M. S.; Morgante, A.; Roy, X.; et al. Determination of the Structure and Geometry of N-Heterocyclic Carbenes on Au(111) Using High-Resolution Spectroscopy. *Chem. Sci.* **2019**, *10*, 930−935.
(55) Berger, R.; Delamarche, E.; Lang, H. P.; Gerber, C.; Gimzewski, J. K.; Meyer, E.; Güntherodt, H.-J. Surface Stress in the Self-Assembly of Alkanethiols on Gold Probed by a Force Microscopy Technique. *Appl. Phys. A: Mater. Sci. Process.* **1998**, *66*, S55−S59.
(56) Godin, M.; Williams, P. J.; Tabard-Cossa, V.; Laroche, O.; Beaulieu, L. Y.; Lennox, R. B.; Grütter, P. Surface Stress, Kinetics, and Structure of Alkanethiol Self-Assembled Monolayers. *Langmuir* **2004**, *20*, 7090−7096.
(57) Marks, L. D.; Peng, L. Nanoparticle Shape, Thermodynamics and Kinetics. *J. Phys.: Condens. Matter* **2016**, *28*, 053001.
(58) Israelachvilli, J. N. *Intermolecular and Surface Forces*; Academic Press: Cambridge, 2011.
(59) Yi, X.; Duan, H. L. Surface Stress Induced by Interactions of Adsorbates and its Effect on Deformation and Frequency of Microcantilever Sensors. *J. Mech. Phys. Solids* **2009**, *57*, 1254−1266.
(60) Wu, F.-F.; Zhang, Z.-F.; Mao, S. Transition of Failure Mode and Enhanced Plastic Deformation of Metallic Glass by Multiaxial Confinement. *Adv. Eng. Mater.* **2009**, *11*, 898−901.
(61) Kruzic, J. J. Bulk Metallic Glasses As Structural Materials: A Review. *Adv. Eng. Mater.* **2016**, *18*, 1308−1331.
(62) Zhang, Q.; Li, N.; Goebl, J.; Lu, Z.; Yin, Y. A Systematic Study of the Synthesis of Silver Nanoplates: Is ″Citrate″ a Magic Reagent? *J. Am. Chem. Soc.* **2011**, *133*, 18931−18939.
(63) Liu, X.; Li, L.; Yang, Y.; Yin, Y.; Gao, C. One-Step Growth of Triangular Silver Nanoplates with Predictable Sizes on a Large Scale. *Nanoscale* **2014**, *6*, 4513−4516.
(64) Hurst, E. C.; Wilson, K.; Fairlamb, I. J. S.; Chechik, V. N-Heterocyclic Carbene Coated Metal Nanoparticles. *New J. Chem.* **2009**, *33*, 1837−1840.
(65) Smith, A. M.; Marbella, L. E.; Johnston, K. A.; Hartmann, M. J.; Crawford, S. E.; Kozycz, L. M.; Seferos, D. S.; Millstone, J. E. Quantitative Analysis of Thiolated Ligand Exchange on Gold Nanoparticles Monitored by ^{1}H NMR Spectroscopy. *Anal. Chem.* **2015**, *87*, 2771−2778.
(66) Hurst, S. J.; Lytton-Jean, A. K. R.; Mirkin, C. A. Maximising DNA Loading on a Range of Gold Nanoparticle Sizes. *Anal. Chem.* **2006**, *78*, 8313−8318.
(67) Plimpton, S. Fast Parallel Algorithms for Short-Range Molecular Dynamics. *J. Comput. Phys.* **1995**, *117* (1), 1−19.
(68) Senftle, T. P.; Hong, S.; Islam, M. M.; Kylasa, S. B.; Zheng, Y.; Shin, Y. K.; Junkermeier, C.; Engel-Herbert, R.; Janik, M. J.; Aktulga, H. M.; et al. The ReaxFF Recative Force-Field: Development, Applications, and Future Directions. *npc Computational Materials* **2016**, *2* (1), 1−14.
(69) van Duin, A. C. T.; Dasgupta, S.; Lorant, F.; Goddard, W. A. ReaxFF: A Reactive Force Field for Hydrocarbons. *J. Phys. Chem. A* **2001**, *105* (41), 9396−9409.
(70) Dulong, C.; Madebene, B.; Monti, S.; Richardi, J. Optimization of a New Reactive Force Field for Silver-Based Materials. *J. Chem. Theory Comput.* **2020**, *16* (11), 7089−7099.
(71) Evans, D. J.; Holian, B. L. The Nose-Hoover Thermostat. *J. Chem. Phys.* **1985**, *83* (8), 4069−4074.

https://doi.org/10.1021/acsnano.2c12497
ACS Nano 2023, 17, 6698−6707